BBA - Molecular and Cell Biology of Lipids 1868 (2023) 159247

Contents lists available at ScienceDirect

BBA - Molecular and Cell Biology of Lipids

journal homepage: www.elsevier.com/locate/bbalip

Lipids uniquely alter rates of insulin aggregation and lower toxicity of amyloid aggregates

Mikhail Matveyenka [a], Stanislav Rizevsky [a,b], Jean-Philippe Pellois [a], Dmitry Kurouski [a,c,*]

[a] Department of Biochemistry and Biophysics, Texas A&M University, College Station, TX 77843, United States
[b] Department of Biotechnology, Binh Duong University, Thu Dau Mot 820000, Viet Nam
[c] Department of Biomedical Engineering, Texas A&M University, College Station, TX 77843, United States

ARTICLE INFO

Keywords:
Neurodegenerative disorders
Protein aggregation
Single-molecule biophysics
Atomic force microscopy
Infrared spectroscopy

ABSTRACT

Amyloid formation is a hallmark of many medical diseases including diabetes type 2, Alzheimer's and Parkinson diseases. Under these pathological conditions, misfolded proteins self-assemble forming oligomers and fibrils, structurally heterogeneous aggregates that exhibit a large variety of shapes and forms. A growing body of evidence points to drastic changes in the lipid profile in organs affected by amyloidogenic diseases. In this study, we investigated the extent to which individual phospho- and sphingolipids, as well as their mixtures can impact insulin aggregation. Our results show that lipids and their mixtures uniquely alter rates of insulin aggregation simultaneously changing the secondary structure of protein aggregates that are grown in their presence. These structurally different protein-lipid aggregates impact cell viability to different extent while using distinct mechanisms of toxicity. These findings suggest that irreversible changes in lipid profiles of organs may trigger formation of toxic protein species that in turn are responsible for the onset and progression of amyloidogenic diseases.

1. Introduction

Amyloid diseases are a large group of severe pathologies that share a common feature, namely the presence of deposits of misfolded proteins within the body [1–3]. Misfolded proteins self-assemble forming oligomeric species that exhibit a large variety of forms and shapes [4,5]. Protein oligomers exert high cell toxicities and play a significant role in the spread of pathologies throughout the body [4,6–11]. They also propagate into insoluble amyloid fibrils, rod-like aggregates with cross-β-sheet secondary structure [10,12]. Cryo-electron microscopy and solid-state nuclear magnetic resonance (ss-NMR) resolved the secondary structure of amyloid fibrils [13–15]. However, the transient nature of oligomers and their morphological heterogeneity limit the use of these classical methods of structural biology for elucidation of the oligomers' structural organization [16]. To overcomes these limitations, several groups proposed an elegant approach that allow for trapping these oligomers [17,18] For instance, Barghorn et al. discovered that stable homogeneous amyloid β1–42 peptide (Aβ1–42) oligomers could be formed if the monomeric peptide was aggregated at low concentrations of sodium dodecyl sulfate (SDS) [19]. Similar findings were reported by Serra-Batiste et al. that observed growth of detergent-stabilized Aβ1–42 oligomers in the presence of dodecyl phosphocholine (DPC) micelles [20]. Although such aggregates exerted cell toxicities, their structural relevance to the native oligomers formed in the absence of detergents remains unclear.

Scanning probe techniques, such as high-speed AFM (HS-AFM) [21,22], as well as optical nanoscopy approaches, such as atomic force microscopy Infrared (AFM-IR) spectroscopy [23–27] and tip-enhanced Raman spectroscopy [28–32] can be used to overcome these limitations. For instance, HS-AFM was able to reveal structural transformations in islet amyloid precursor peptide (IAPP), $A\beta_{1-42}$ and α-synuclein (α-Syn) that lead to fibril formation [21,33,34]. These proteins that are directly linked to diabetes type 2, Alzheimer's and Parkinson diseases, respectively. Furthermore, HS-AFM revealed two aggregation mechanisms of $A\beta_{1-42}$ that led to formation of straight and spiral fibrils [22]. Using NMR, AFM, mass spectroscopy, and computational simulations, Wei et all found that in solution IAPPs rapidly aggregated into transient dimers and trimers that slowly propagate into higher-order spherical oligomers and elongated fibrils [35]. These findings can help to find targeted therapeutic strategies to block protein aggregation at the early stages.

In AFM-IR, a metalized scanning probe is positioned above the

* Corresponding author at: Department of Biochemistry and Biophysics, Texas A&M University, College Station, TX 77843, United States.
E-mail address: dkurouski@tamu.edu (D. Kurouski).

https://doi.org/10.1016/j.bbalip.2022.159247
Received 30 June 2022; Received in revised form 14 September 2022; Accepted 2 October 2022
Available online 20 October 2022

sample of interest that is illuminated by pulsed tunable IR light [36–38]. IR-induced thermal expansions in the sample are recorded by the scanning probe [39,40]. If a resonance frequency of the scanning probe matches the laser frequency, appearing resonance effect enables single-monolayer and even single-molecule sensitivity [41,42]. This high sensitivity and nanometer spatial resolution made AFM-IR highly attractive for structural analysis of wide variety of samples: amyloid fibrils, [23,25,26,43–45] plant epicuticular waxes [46,47], polymers [48], malaria infected blood cells [49], meteorites [50], bacteria [51–53], liposomes [54] and polycrystalline perovskite films [55].

Using AFM-IR, our group was able to determine structural changes that take place upon aggregation of α-Syn [27]. Zhou and co-workers found that α-Syn forms two types of oligomers at the early stages of aggregation: one dominated by α-helical/unordered structure and one mostly composed of antiparallel- and parallel-β-sheet. The first type of oligomers remain unchanged during the course of protein aggregation, whereas antiparallel β-sheet rearrange into parallel-β-sheet secondary in the second type of oligomers upon their propagation into fibrils [27].

A growing body of evidence suggests that a large number of biological molecules can uniquely alter rates of protein aggregation and modify toxicity of oligomers and fibrils.[56–58] For instance, Cataldi and co-workers showed that 3,4-dihydroxyphenylacetaldehyde, a product of dopamine oxidation, alters the secondary structure of amyloid β oligomers and increases their toxicity significantly [56]. Galvagnion and co-workers found that lipids either accelerate or decelerate the rate of α-Syn aggregation. This effect is determined by the chemical structure of the lipid, as well as lipid to protein ratio [59–61]. Our group found that lipids not only alter the rates of α-Syn aggregation but also uniquely modify secondary structure of protein oligomers [5]. Similar observations were reported by Zhang et al. for IAPP [62]. Specifically, the researchers showed that low levels of anionic lipids promoted IAPP aggregation and enhanced membrane permeabilization potential of these aggregates. At the same time, zwitterionic lipid did not alter the rate of IAPP aggregation, whereas cholesterol at or below physiological levels significantly decelerated IAPP amyloid formation, as well as lowered the propensity of IAPP aggregates to cause membrane leakage. Lipids can also uniquely alter the structure of amyloid β1–40 (Aβ1–40) aggregates [63]. A critical question is whether this lipid-mediated effect on structure and aggregation kinetics is unique to α-Syn, IAPP and Aβ1–40 or whether it is a general phenomenon applicable to a large group of amyloid-associated proteins.

Insulin is a small hormone that regulates glucose metabolism. If present at high concentrations, insulin forms oligomers and fibrils [30,64]. Insulin aggregation is associated with diabetes type 2, a severe pathology characterized by a suppressed response of cells to insulin [65]. As a result, an overproduction of insulin takes place in the pancreas, triggering insulin misfolding and aggregation. Similar processes are observed upon injection-induced amyloidosis [66,67]. In this case, injection if a high local concentration of insulin in the skin dermis and subcutaneous fat triggers the formation of fibrils [68]. These fibrils in turn may trigger the aggregation of other proteins, a phenomena which results in systemic amyloidosis [69]. In the subcutaneous fat, injected insulin is exposed to lipids, including the phospholipids, ceramides and sphingolipids found in the membranes of cells [70]. Phosphatidylcholine (PC), phosphatidylserine (PS), cardiolipin (CL), ceramide (CER) and sphingomyelin (SM) also occupy significant part of the lipid membranes in most of eucaryotic cells [70–73]. Specifically, PC is the most observed lipid that takes up to 47 % of the membranes, whereas the ~10 % of the organelle and plasma membranes are occupied by PS. Although the contributions of CER and SM are smaller, these lipids take up to 6 % and 4 % of eukaryotic plasma membranes, respectively. CL is unique to the inner mitochondrial membranes where it where it constitutes about 20 % of all present lipids. It should be noted that all chosen lipids for this work possessed C_{16}-C_{18} saturated fatty acids (FA). Although lipids with unsaturated FA also play an important role in membrane biophysics, elucidation of their impact on insulin aggregation is the subject for a separate study. Therefore, in our study we tested the effect of these lipids, as well as their mixtures, on insulin aggregation. Our findings show that lipids uniquely alter rates of insulin aggregation. Furthermore, lipids modify the morphology and secondary structure of insulin aggregates. Such aggregates exert significantly lower cell toxicities than insulin aggregates grown in the lipid-free environment.

2. Results

2.1. Kinetics of insulin aggregation

We first examined the extent to which lipids can alter the lag-phase and rate of insulin aggregation. For this, insulin was mixed in 1:1 M ratio with PC, PS, CL, SM and CER. The solutions were mixed with ThT and kept at 37 °C under 510 rpm agitation. Insulin aggregation in the lipid-free environment had a well-defined lag-phase that was followed by a rapid increase in the ThT intensity, which indicated a formation of protein aggregates, Fig. 1. We found that lipids can either shorten or delay the lag-phase (t_{lag}) of insulin aggregation (t_{lag} = 14.4 ± 0.8 h), Table S1 and Fig. S1. Specifically, CL (t_{lag} = 3.2 ± 0.5 h), CER (t_{lag} = 7.7 ± 0.5 h) and PS (t_{lag} = 8.2 ± 1.0 h) substantially shortened, whereas SM delayed the lag-phase (t_{lag} = 23.5 ± 1.0 h). We also observed no changes in ThT intensity for Ins:PC, which suggests that PC strongly inhibits insulin aggregation. These findings show that lipids can both shorten and delay the lag-phase of insulin aggregation.

Next, we aimed to reveal the extent to which the effect of CL, which caused the most substantial shortening of the t_{lag}, can be reduced by PC, the lipid that strongly inhibited fibril formation. For this, we aggregated insulin the presence of a mixture of PC and CL at 50:50 and 80:20 M ratios (Ins:PC:CL (1:0.5:0.5) and Ins:PC:CL (1:0.8:0.2), respectively). If t_{lag} for Ins:CL was 3.2 ± 0.5 h, t_{lag} for Ins:PC:CL (1:0.5:0.5) was 6.8 ± 1.7 h. These findings confirm our hypothesis that presence of PC inhibits acceptation effect of CL on insulin aggregation. We also found that an increase in the relative concentration of PC relative to CL (Ins:PC:CL (1:0.8:0.2)), similarly to PC itself, resulted in the full inhibition of insulin fibril formation.

We have also found that lipids can uniquely alter the rate of insulin aggregation. We found that CL ($t_{1/2}$ = 6.4 ± 0.3 h), CER ($t_{1/2}$ = 11.4 ± 1.0 h), PS ($t_{1/2}$ = 10.9 ± 0.6 h) and Ins:PC:CL (1:0.5:0.5) ($t_{1/2}$ = 9.5 ± 2.9 h) substantially accelerated the rate of protein aggregation (Insulin $t_{1/2}$ = 18.1 ± 0.4 h), Table S1 and Fig. S1. However, SM ($t_{1/2}$ = 25.5 ± 0.4 h), on the opposite, decelerated the rate of insulin aggregation. These findings show that lipids uniquely alter both a lag-phase and the rate of insulin aggregation.

2.2. Morphological analysis of insulin aggregates

We utilized AFM to investigate a morphology of insulin aggregates grown in the presence of lipids, as well as in the lipid-free environment, Fig. 2. We found that in the lipid-free environment (Ins), insulin formed prolong fibrillar assemblies with a large distribution of lengths that had on average 12 nm in height, Fig. 2 and Figs. S2-S3. In the presence of CL (Ins:CL), insulin aggregation yielded short (30–60 nm) spherical aggregates and ~ 200 nm long fibrils that had 6–8 nm in height. Similar aggregates have been observed for Ins:CER, Ins:PS and Ins:SM (6–12 nm in height). In the presence of PC, insulin formed only small (4–6 nm in height) oligomers. Aggregates with similar morphologies and dimensions were found for Ins:PC:CL (1:0.8:0.2) together with short, fibril-like structures. An increase in the concentration of CL relative to PC (Ins:PC:CL (1:0.5:0.5)), resulted in formation of short (40–70 nm) spherical aggregates and 90–160 nm long fibrils that have ~12 nm in height. These aggregates had similar topologies with those formed by insulin in the presence of CL itself. Summarizing, we can conclude that in the lipid-free environment, insulin aggregates into long fibrils, whereas in the presence of PS, CL, SM and CER short fibrillar species

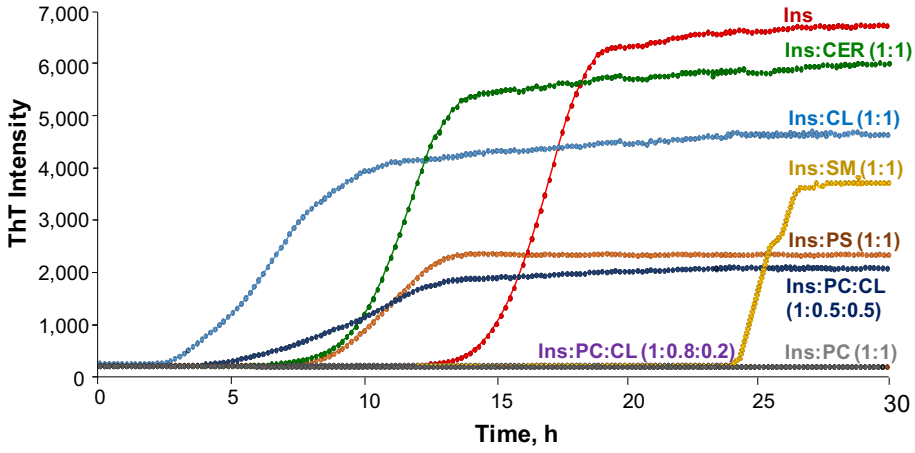

Fig. 1. Lipids uniquely alter the rate of insulin aggregation. Averages of triplicates of ThT aggregation kinetics of insulin in the lipid-free environment (Ins) and in the presence of CL, CER, PS, PC and SM at 1:1 molar ratio, as well as in the presence of lipid mixtures PC:CL at 1:1 and 0.8:0.2. For Ins, 400 μM of protein was dissolved in 1xPBS with 2 mM of ThT; pH adjusted to pH 3.0. For Ins:CL, Ins:CER, Ins:PS and Ins:SM, as well as for Ins:PC:CL (1:0.5:0.5) and Ins:PC:CL (1:0.8:0.2), 400 μM of insulin was mixed with an equivalent concentration of the corresponding lipid; pH was adjusted to pH 3.0. All samples were kept at 37 °C under 510 rpm for 24 h.

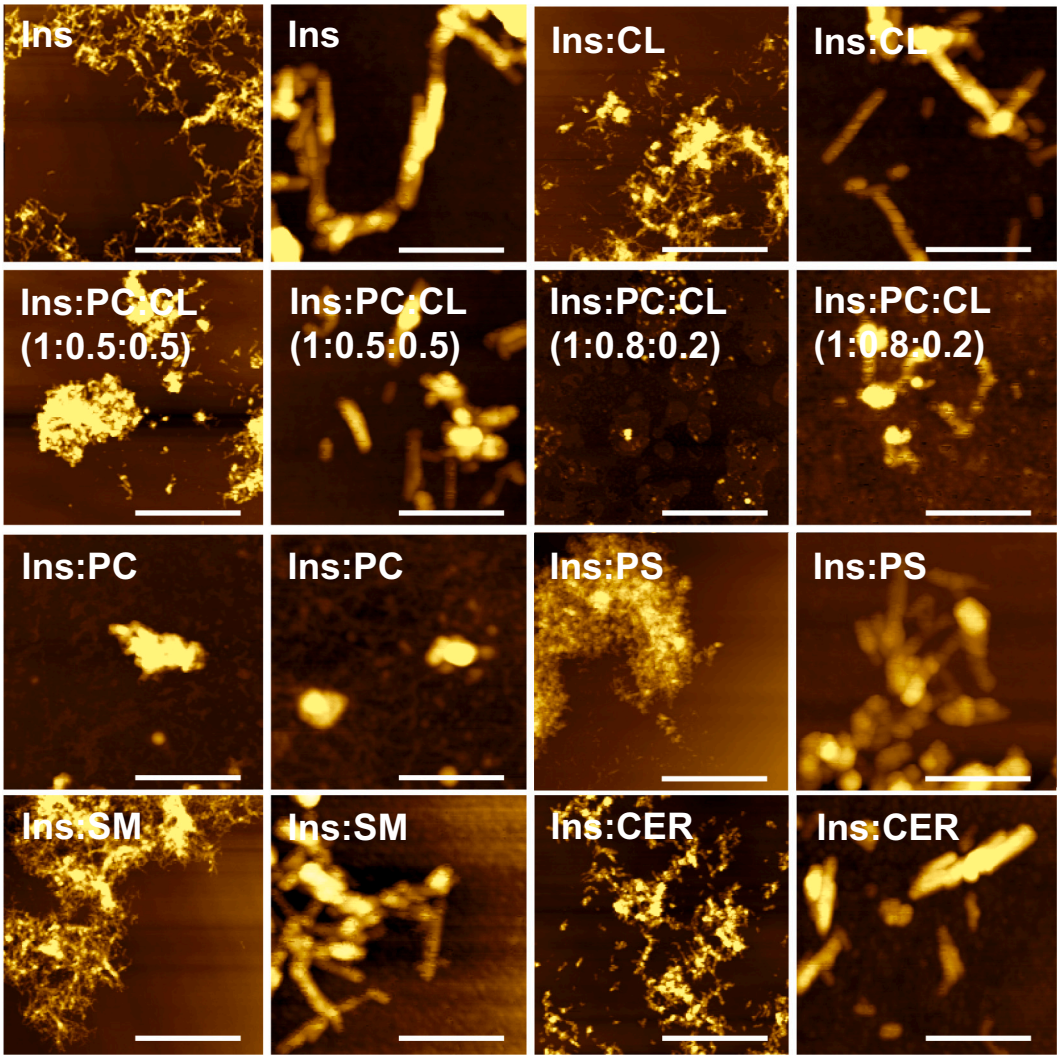

Fig. 2. Lipids uniquely alter morphologies of insulin aggregates. AFM images of Ins aggregates, Ins:PS, Ins:PC, Ins:CL, Ins:PC:CL (1:0.5:0.5), Ins:PC:CL (1:0.8:0.2), Ins:SM and Ins:CER. After 24 h of incubation of insulin (400 μM) with and without lipids at 37 °C under 510 rpm, sample aliquots were diluted with 1xPBS pH 3.0 and deposited onto pre-cleaned silicon wafer. AFM imaging was performed in tapping mode. Scale bars are 2 μm for the first and third rows and 200 nm for the second and forth rows.

together with spherical oligomers are grown. In the presence of PC, insulin forms only small oligomers. This inhibitory activity of PC is also evident from a comparison of aggregates observed for Ins:PC:CL (1:0.5:0.5) and Ins:PC:CL (1:0.8:0.2). An increase in the concentration of PC in the lipid mixture decreases the yield of fibrils and increases the amount of spherical oligomers. These findings show that lipids either significantly alter morphologies of protein fibrils (CL, PS, SM and CER) or strongly inhibit fibril formation (PC).

2.3. Structural characterization of protein aggregates

We utilized CD and ATR-FTIR to examine the secondary structure of insulin aggregates grown in the presence of lipids, as well as in the lipid-free environment. CD spectra of Ins, Ins:CER, Ins:PS, Ins:CL, Ins:SM, as well as Ins:PC:CL (1:0.5:0.5) exhibited a trough at ~225 nm, which indicates the dominance of β-sheet in their secondary structure, Fig. 3 and Table S2 [74,75]. However, Ins:PC and Ins:PC:CL (1:0.8:0.2) had drastically different CD spectra with two troughs at 209 and 222 nm. Such spectra are characteristic to proteins with a mixture of α-helical and unordered secondary structures, Fig. S2 [74,75].

ATR-FTIR spectra collected from Ins:PC and Ins:PC:CL (1:0.8:0.2) aggregates exhibited the amide I at ~1657 cm^{-1}, Fig. 3. This observation demonstrates that Ins:PC and Ins:PC:CL (1:0.8:0.2) have primarily α-helix and unordered protein secondary structure. [76,77] In the spectra collected from Ins:CER, Ins:PS, Ins:CL, Ins:SM, as well as Ins:PC:CL (1:0.5:0.5), the amide I was centered at ~1631 cm^{-1}, which indicates the dominance of parallel β-sheet secondary structure in these protein aggregates [76,78]. We have also found that ATR-FTIR spectrum of Ins aggregates exhibited amide I at 1628 cm^{-1}. This finding points on the substantial structural difference between the parallel β-sheet secondary structure in insulin aggregates grown in the lipid-free environment and the aggregates grown in the presence of lipids. Finally, we observed a shoulder at 1657 cm^{-1} in the amide I region of the spectra collected form Ins, Ins:CER, Ins:PS, Ins:CL, Ins:SM, as well as Ins:PC:CL (1:0.5:0.5). This points out on the presence of unordered protein secondary structure in all insulin aggregates [27,79].

One may expect that differences in the structural organization between aggregates that were grown in the presence and absence of lipids

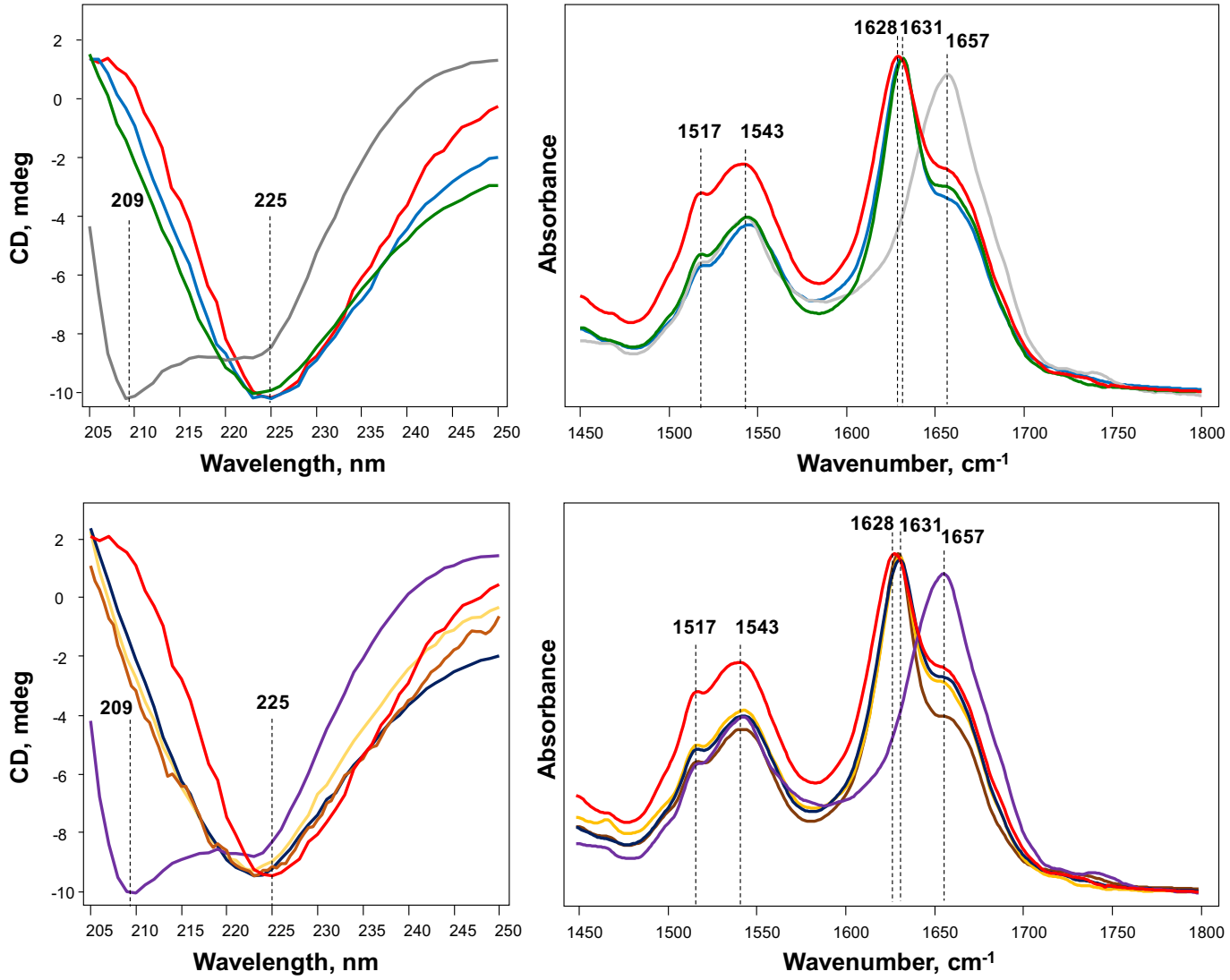

Fig. 3. Structural analysis of insulin aggregates. CD (left) and ATR-FTIR (right) spectra of insulin aggregates (Ins) grown in the lipid-free environment (red), Ins:CER (green), Ins:CL (blue), Ins:PC (gray), Ins:SM (yellow), Ins:PS (brown), Ins:PC:CL (1:0.5:0.5, navy) and Ins:PC:CL (1:0.8:0.2, purple). After 24 h of incubation of insulin (400 μM) with and without lipids at 37 °C under 510 rpm, triplicates of samples were diluted with 1xPBS pH 3.0 and placed into quartz cuvette (CD) or directly deposited onto ATR crystal (ATR-FTIR) and dried under room temperature. For each of the presented traces, three independent CD or ATR-FTIR measurements were averaged. (For interpretation of the references to colour in this figure legend, the reader is referred to the web version of this article.)

can arise from a presence of lipids in such aggregates. ATR-FTIR is insufficient to examine the presence of lipids in the aggregates because if lipid vibrations are observed in the corresponding spectra, we cannot unambiguously determine whether lipids are integrated in the aggregates or simply co-present with such protein aggregates. To overcome this limitation, we used AFM-IR. AFM-IR allows for a direct visualization individual protein aggregates simultaneously enabling their structural analysis. [5,25,26,80]

AFM-IR spectra collected from individual protein aggregates that were grown in the presence of lipids exhibited vibrational bands centered ~800 and 1000–1200 cm^{-1}, Fig. 4. These vibrational bands correspond to C—H and PO_2^- vibration respectively [80]. We have found that Ins:PS, Ins:PC, Ins:CER and Ins:CL exhibited very strong intensities of ~800 and 1000–1200 cm^{-1} bands. This finding point on the presence of a significant amount of lipids in their structure. We also found that intensities of 1000–1200 cm^{-1} bands were substantially lower in the spectra collected from Ins:PC:CL (1:0.5:0.5) and Ins:PC:CL (1:0.8:0.2) comparing to the intensities of these bands in the spectra collected from Ins:PS, Ins:PC, Ins:CER and Ins:CL. Previously, we have demonstrated that intensity of PO_2^- vibration directly depends on the local environment of the lipid head groups. Thus, our AFM-IR results show that the underlying lipid-protein structure of Ins:PC:CL (1:0.5:0.5) and Ins:PC:CL (1:0.8:0.2) are drastically different from both Ins:PC and Ins:CL.

AFM-IR analysis of Ins:SM showed significant variability in the intensity of the acquired spectra. In some of the collected spectra intensities of ~800 and 1000–1200 cm^{-1} vibrations were low whereas in other spectra these bands very found to be very intense. Such fluctuations in the intensities of the vibrational bands point on structural

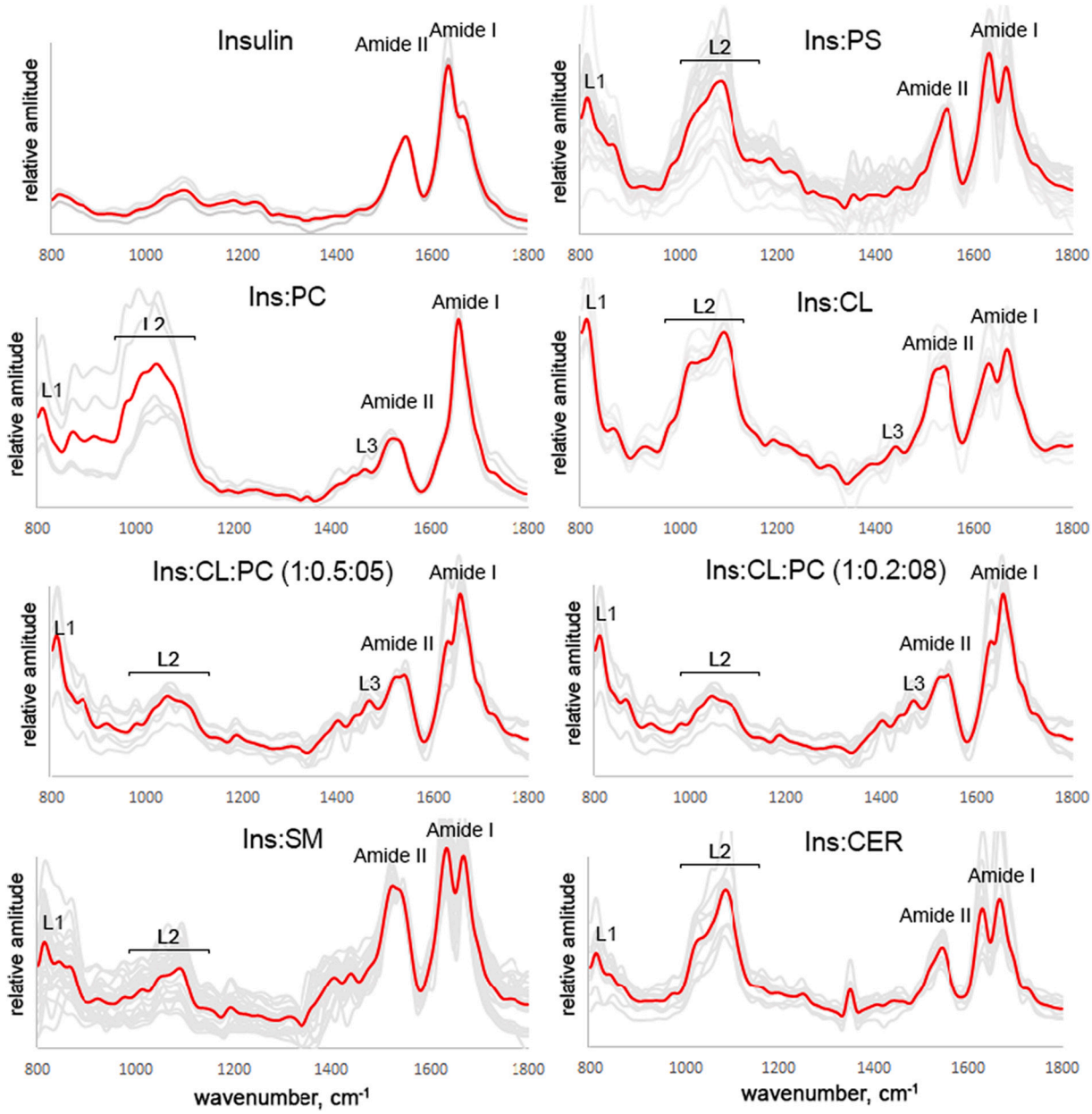

Fig. 4. Nanoscale analysis of lipid content of insulin aggregates. AFM-IR spectra of insulin aggregates grown in the absence of lipids (Ins) and in the presence of PS, PC, CL, as Ins:PC:CL (1:0.5:0.5), as Ins:PC:CL (1:0.8:0.2), SM and CER. Spectra collected from individual aggregates are in gray, whereas the corresponding average spectra are in red. After 24 h of incubation of insulin (400 μM) with and without lipids at 37 °C under 510 rpm, sample aliquots were diluted with 1xPBS pH 3.0 and deposited onto pre-cleaned silicon wafer. AFM-IR analysis was performed in contact mode. At least 30–40 individual aggregates were analyzed for each sample. (For interpretation of the references to colour in this figure legend, the reader is referred to the web version of this article.)

heterogeneity of Ins:SM aggregates. We found that spectra predominantly collected from small spherical aggregates exhibit intense ~800 and 1000–1200 cm^{-1} vibrations, whereas AFM-IR spectra collected from fibrils often showed low intensities in these regions. This observation shows that lipids primarily present in the pre-fibrillar aggregates and are rarely observed in fibrils. This finding is in a good agreement with previously reported results by our group, as well as other researchers. Specifically, Galvagnion and co-workers hypothesized that proteins utilize lipid layers for their assembly [60,81]. Using AFM-IR, our group showed that such assembly is driven by lipids that form complexes with proteins. [5] Such complexes yield structurally and morphologically different fibrils. AFM-IR results reported in the Fig. 4 confirm that lipids present in all of the analyzed insulin aggregates that were grown in the presence of lipids. We infer that presence of lipids in such aggregates and unique lipid-protein complex play a critically important role for their toxicity.

2.4. Toxicity of insulin aggregates

We utilize mice midbrain N27 cell line and a set of toxicity assays to examined the relationship between oligomer structure and toxicity. Amyloid aggregates are thought to exert toxicities by enhancing ROS production and inducing the mitochondrial dysfunction in cells. [4,56] Therefore, we examined general cell toxicity of insulin aggregates, as well as investigated the extent to which these structures are engaged in ROS production and mitochondrial dysfunction of cells, Fig. 5.

LDH test indicated that Ins:CL, Ins:PC:CL (1:0.5:0.5), Ins:PC:CL (1:0.8:0.2), Ins:PC, Ins:PS and Ins:SM exhibited significantly lower cell toxicities compared to insulin aggregates grown in the lipid-free environment (Ins), Fig. 5. Specifically, toxicity of Ins:CL and Ins:PC:CL (1:0.5:0.5) was twice, whereas toxicity of Ins:PS, Ins:PC and Ins:PC:CL (1:0.8:0.2) was more than three times lower than toxicity of Ins aggregates. Ins:CER exhibited similar cell toxicity to Ins aggregates. Importantly, lipids themselves did not exert any significant cell toxicity.

The results of ROS test were consistent with the results of the discussed above LDH levels that were observed upon the exposure of N27 cell to the insulin aggregates that grown in the lipid-free and lipid-rich environments. We found that Ins aggregates yield significantly higher ROS levels compared to the aggregates grown in the presence of lipids. We have also found that Ins:PC:CL (1:0.8:0.2) and Ins:PC caused the lowest ROS production. ROS response increased from Ins:PC:CL (1:0.5:0.5) to Ins:CL, Ins:PS, Ins:SM and Ins:CER.

We also utilized the JC-1 dye, a probe of mitochondrial membrane potential, to examine the mitochondrial dysfunction caused by insulin aggregates. It was found that insulin aggregates grown in the lipid-free environment cause significantly higher mitochondrial dysfunction comparing to the protein aggregates grown in the absence of lipids. Thus, if grown in the presence of lipids, insulin aggregates will exert substantially lower ROS and mitochondrial dysfunction. We have also found that CL, PC:CL (1:1), PC:CL (1:4) and SM exert small but noticeable mitochondrial dysfunction. Overall, our results show that lipids uniquely alter the toxicity of insulin aggregates. Furthermore, the structure and corresponding toxicity of such aggregates is governed by the chemical structure of the lipid.

2.5. Mechanism of insulin aggregates' toxicity

Protein aggregates can permeabilize the plasma membrane of cells directly or alternatively enter cells *via* endocytosis. In the former case, amyloid aggregates damage the cell plasma membrane, and this can cause a cell death. [82] In the latter case, protein aggregates accumulate inside endosomes. The aggregates can subsequently be exocytosed to return to the cell's exterior. However, aggregates may also damage endosomal membranes and leak into the cytosol. They may thus use this route to induce ROS and mitochondrial dysfunction [83,84]. We performed a set of biochemical assays to determine whether insulin aggregates are endocytosed by cells and whether they cause damage to the endosomal membranes. Such damages initiate endosomal repair, clearance of damaged endosomes by autophagy and *de novo* biogenesis of organelles [85].

To establish relationships between insulin aggregates and endosomal membrane damage, the probes Chmp1-EGFP, Gal3-EGFP, and TFEB-EGFP were used. Chmp1 proteins bind to membranes of damaged endosomes that exhibit Ca^{2+} leakage into the cytosol engaging ESCRT-III complex in membrane repair processes, [85–87] Scheme 1. Endosomal damage can also expose luminal β-galactosides to the cytosol. Cytosolic Gal3 binds to exposed β-galactosides, thereby initiating autophagy, [85,88] Scheme 1. Chmp1-EGFP and Gal3-EGFP construct were transiently transfected into cells and endosomal membrane damage was detected by quantifying the localization of Chmp1-EGFP or Gal3-EGFP by fluorescence microscopy. A diffuse and cytosolic distribution of Chmp1/Gal3 is observed in the absence of endosomal while Chmp1/Gal3-EGFP puncta form when endosomes are damaged. Finally, TFEB is a transcription factor that regulates lysosomal biogenesis and autophagy [89–91]. Activation of TFEB is linked to endosomal Ca^{2+} efflux, activation of the phosphatase calcineurin, dephosphorylation of TFEB, and subsequent translocation of the transcription factor to the nucleus, Scheme 1. [85] In turn, nuclear TFEB activates a transcriptional program that induce *de novo* biogenesis of endosomal organelles. Therefore, cell transfected with TFEB-EGFP were used to monitor the cytoplasm to nucleus translocation of the transcription factor upon exposure to insulin aggregates.

We found that insulin aggregates grown in the presence and absence of lipids cause damage of endosomal membranes, as measured by Chmp1, Gal3 and TFEB, Fig. 6 and Fig. S4. The extent of endosomal damage directly depends on the structure of the aggregates. Specifically, Ins:PS causes higher Ca^{2+} leakages, endosomal repair (Chmp1b) and *de novo* biogenesis (TFEB) of endosomes comparing to other insulin aggregates. At the same time, Ins:CL and Ins:PC:CL (1:0.5:0.5) induce the lowest Ca^{2+} leakages and endosomal repair (Chmp1b). We also found that Ins and Ins:PS induce very little endosomal autophagy (Gal3), whereas Ins:CL, Ins:PC:CL (1:0.5:0.5) and Ins:PC primarily disrupt endosomes using Gal3 pathway. These findings show that insulin aggregates cause damages of endosomal membranes inducing their repair and *de novo* biogenesis.

3. Discussion

Abrupt insulin aggregation is the underlying molecular cause of injection amyloidosis, a severe pathology that arises from the injection of insulin in the skin dermis and subcutaneous fat layer [66,67]. Injections cause a local increase in the concentration of insulin, which, in turn, triggers protein aggregation. Insulin aggregates can induce abrupt aggregation of a large number of proteins present in the body, which results in systemic amyloidosis [69]. As was previously demonstrated by Kurouski and co-workers, insulin aggregation at pH below 2 resulted in formation of tape-like fibrils, whereas at pH above 2, insulin formed left-twisted fibrils [76]. It was also found that these tape-like and twisted fibrils had distinctly different supramolecular chirality [76].

Lipids are one of the most abundant classes of biological molecules in subcutaneous fat and cell membranes. Our results show that lipids drastically alter insulin stability either accelerating or decelerating its aggregation. We found that phospholipids with net negative charges, such as CL (net charge is −2) or PS (net charge is −1) strongly accelerate insulin aggregation. Zwitterion lipids, such as SM and PC either decelerate (SM) or strongly inhibit (PC) insulin aggregation. Interestingly that CER that possesses no charges at neutral pH also accelerates insulin aggregation. This finding suggests that both charge and chemical structure of the lipid play an important role in lipid-protein interactions that trigger or inhibit insulin aggregation.

It should be noted that not only the charge of lipids, but also curvature of the lipid vesicles can play an important role in protein-lipid

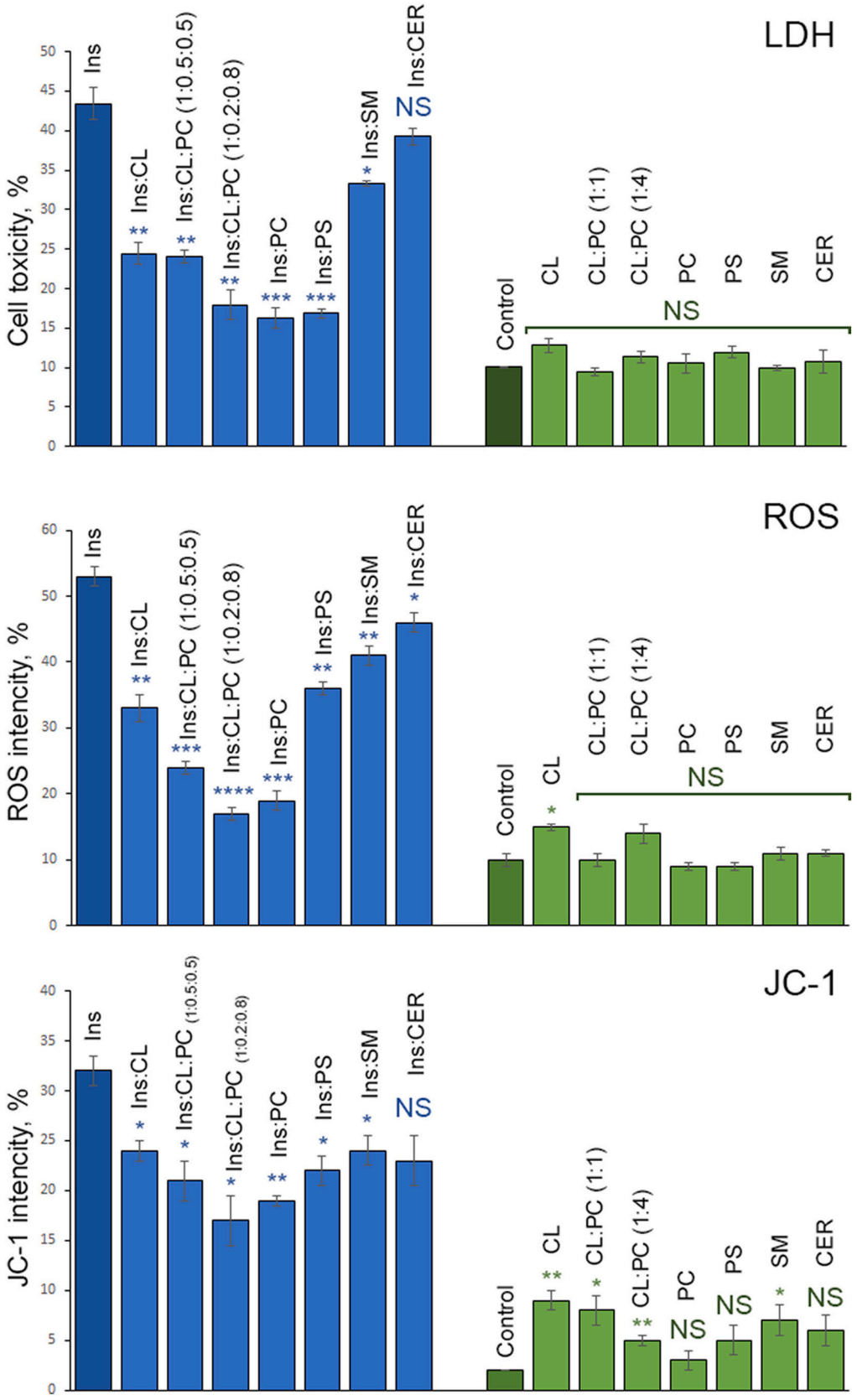

Fig. 5. Insulin aggregates grown in the presence of lipids are less toxic than the aggregates grown in the lipid-free environment. Histograms of LDH (top), ROS (middle) and JC-1 (bottom) toxicity assays of Ins, Ins:CL, Ins:CL:PC (1:0.5:0.5), Ins:CL:PC (1:0.2:0.8), Ins:PC, Ins:PS, Ins:SM and Ins:CER, as we as CL, CL:PC (1:1), CL:PC (1:4), PC, PS, SM and CER. After 24 h of incubation of insulin (400 μM) with and without lipids at 37 °C under 510 rpm, sample triplicates were exposed to mice midbrain N27 cells for 48 h. For each of the presented results, three independent measurements were made.

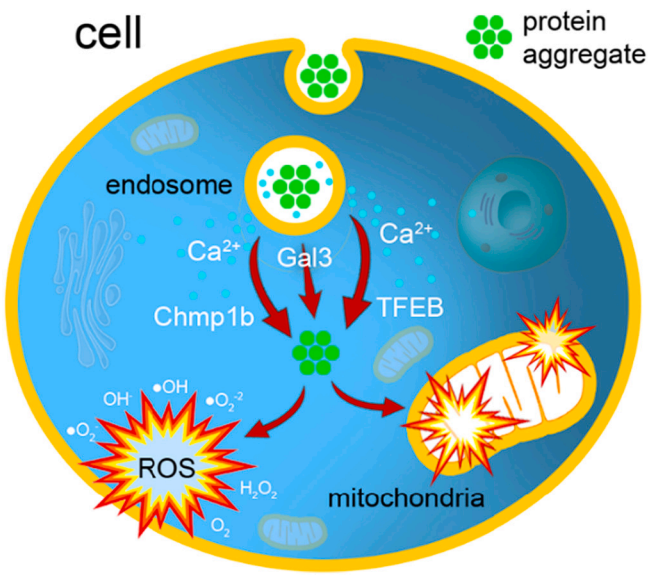

Scheme 1. Mechanism of cell toxicity exerted by insulin aggregates.

interactions that can alter the rates of protein aggression [92,93]. For instance, Terakawa and co-workers demonstrated that small unilamellar vesicles (SUVs) enable much faster aggregation of amyloid β1–40 peptide comparing to large unilamellar vesicles (LUVs) with the same lipid composition [94]. The researchers inferred that this effect originates from a higher level of defects of lipids in SUVs comparing to LUVs. Consequently, lipids in these defects are more accessible to proteins that localize on the surface of the vesicles. Considering these observations, all phospholipids utilized in our study were assembled into LUVs with the same (~100 nm) vesicle diameter prior to mixing with insulin.

Lipid-protein interactions are developed between charged amino acid residues of proteins and polar head groups of lipids. For instance, lysine and glutamic acid residues on N-terminus (amino acids 1–60) of α-Syn exhibit strong electrostatic interactions with headgroups of phospholipids that triggers α-Syn aggregation [95]. NMR and fluorescence methods also revealed that lipid-protein interactions are facilitated by hydrophobic interactions between non-polar amino acid residues of the protein and fatty acid tails of lipids [96,97]. Our findings show that lipid-protein interactions with PC inhibit fibril formation yielding only small oligomeric species that are highly rich with unordered protein secondary structure. These oligomeric structures exhibit low cell toxicity. Insulin interactions with SM, although decelerate its aggregation, yield β-sheet-rich fibril-like structures that are highly toxic to cells. Similar β-sheet-rich fibril aggregates are observed for Ins:CER, Ins:PS and Ins:CL. However, toxicities of these morphologically similar aggregates are significantly different. Furthermore, such aggregates exhibit distinctly different mechanisms of cell damage. These findings suggest that differences in the secondary structure itself may not be sufficient to explain differences in the toxicities of amyloid aggregates.

Our previous findings and experimental results presented in this study show that lipids become integrated in protein aggregates that form in their presence [5,98–101]. These conclusions are based on observed by AFM-IR vibrations of PO^{2-} of lipid head-groups in the spectra collected from both α-Syn [5,98] and insulin [99–101] aggregates formed at different stages of protein aggregation. Specifically, Rizevsky and co-workers found that insulin oligomers grown in the presence of both PC and CL possessed the corresponding lipid molecules in their structure [99]. It was also found that insulin filaments and fibrils grown in the presence of these phospholipids possessed significantly lower amount of lipids. Furthermore, it was found that in the presence of both phospholipids, insulin preferably bound PC rather than CL [99]. These results suggested that drastic differences in toxicities of β-sheet-rich fibril structures were likely determined by the chemical structure of lipid-protein complex present in such aggregates.

An uptake of amyloid aggregates by cells typically occurs by their endocytosis. Our findings show that insulin aggregates damage endosomes triggering a cascade of endosomal repair mechanisms, Scheme 1. Endosomal damage, in turn, induces Ca^{2+} leakage into cytosol. This disruption of Ca^{2+} homeostasis is a likely pathomechanism of cell apoptosis that compromises living systems in the context of aging. In addition to the Ca^{2+} leakage, degradation of endosomes may lead to the escape of the aggregates into the cytosol where they induce ROS production and cause mitochondrial damage. These results are in a good agreement with recently reported findings by Matveyenka and co-workers [102]. Specifically, it was demonstrated that insulin aggregates grown in the lipid-free environment and in the presence of lipids caused irreversible damage of cell endoplasmic reticulum (ER), an important cell organelle used for calcium storage, protein synthesis and folding. Specifically, amyloid-induced ER damage activates the unfolded protein response (UPR) in the cell, which, in turn, suppresses protein expression and increases chaperon activity. Thus, one can expect that with an enhanced ROS levels and mitochondrial damage, cells fail to mitigate the ER stress and restore normal cell physiology, which ultimately causes their death.

4. Conclusions

Our experimental findings show that lipids uniquely alter both the lag-phase and rate of insulin aggregation. We also found that in the presence of lipids, insulin forms structurally and morphologically different aggregates that have significantly lower cell toxicities then fibrils grown in the lipid-free environment. We observed a direct relationship between presence of β-sheer secondary structure and cell toxicity. We also found that a level of cell toxicity, ROS production and mitochondrial damage is dictated by the lipid-protein complex that is different for different lipids.

It should be noted that the reported in this work results only revealed biophysical effects of individual lipids on the rates of insulin aggregation, as well as on the structure and corresponding toxicity of insulin aggregates. We expect that these results can be used to model the effects of these lipids in the context of lipid membranes to establish the connection between change in the lipid profile of cell membranes and neurodegeneration. Nevertheless, other important chemical and physical factors such as lipid composition of membranes, membrane defects and curvatures, should be considered to establish the relationship between a change in the lipid profiles and neurodegeneration.

5. Experimental section

5.1. Materials

Bovine insulin was purchased from Sigma-Aldrich (St. Louis, MO, USA), 1,2-ditetradecanoyl-sn-glycero-3-phospho-L-serine (DMPS or PS), 1,2-Dimyristoyl-sn-glycero-3-phosphocholine (DMPC or PC), 1′,3′-bis [1,2-distearoyl-sn-glycero-3-phospho]-glycerol (18:0 cardiolipin (CL)), sphingomyelin (SM) and ceramide (CER) were purchased from Avanti (Alabaster, AL, USA).

5.2. Liposome preparation

DMPS, DMPC and CL large unilamellar vesicles (LUVs) were prepared accordingly to the method reported by Galvagnion et al. [103] Briefly, 0.6 mg of the lipid were dissolved in 2.6 mL of phosphate buffered saline (PBS) pH 7.4. Lipid solutions were heated in water bath to ~50 °C for 30 min and then placed into liquid nitrogen for 3–5 min. This procedure was repeated 10 times. After this, lipid solutions were passed 15 times through a 100 nm membrane that was placed into the extruder (Avanti, Alabaster, AL, USA). LUV sizes were determined by

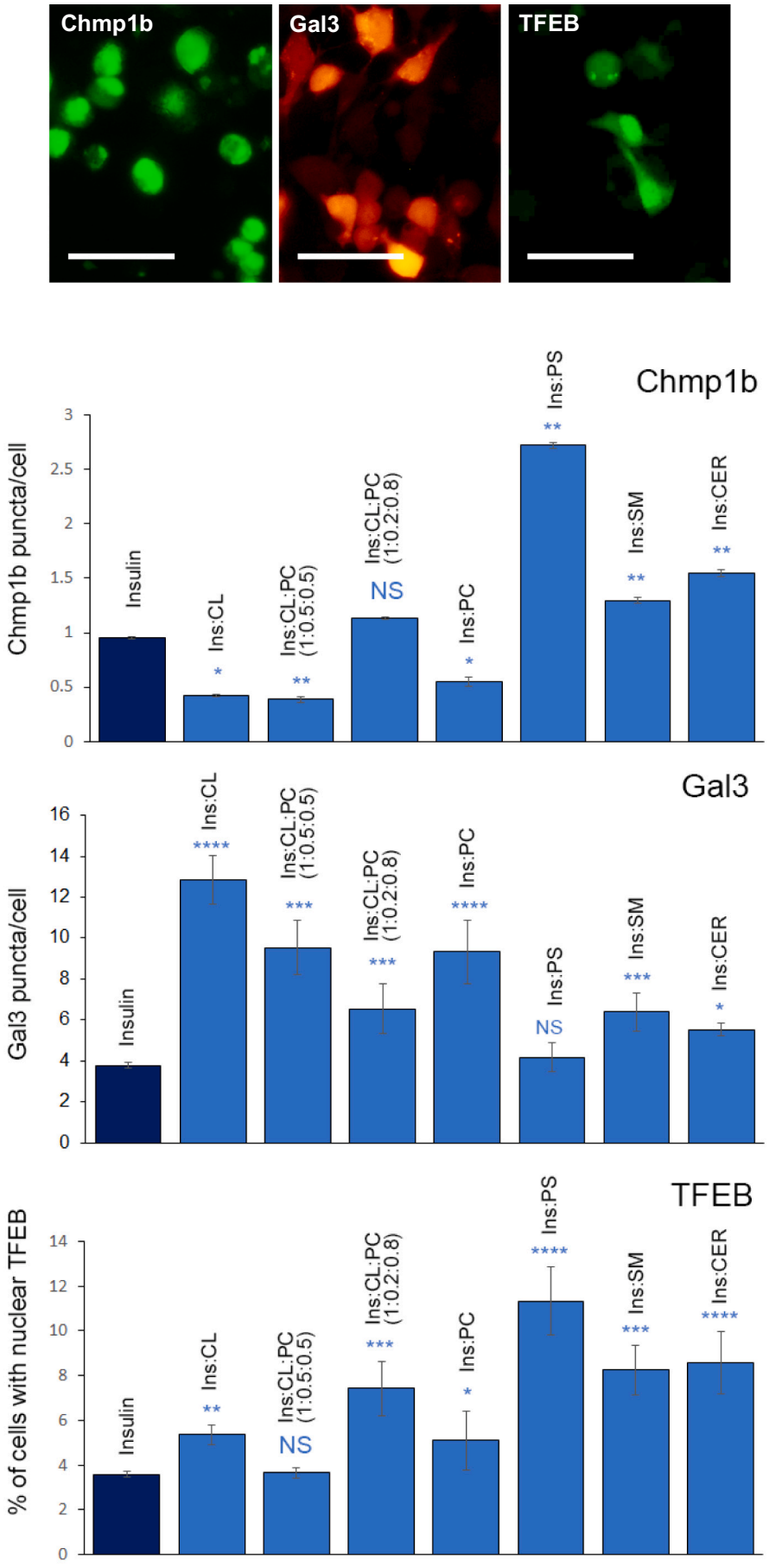

Fig. 6. Endosomal damage induced by insulin aggregates. Representative fluorescence of images of cells exposed to insulin aggregates (top). Images are pseudo-colored green for Chmp1b and TFEB, and red for Gal3. After 24 h of incubation of insulin (400 μM) with and without lipids at 37 °C under 510 rpm, sample triplicates were exposed to HEK 293 T cells with previously transfected with Chmp1b, TFEB, and Gal3 plasmids. Scale bar is 50 μm. Histograms of fluorescent puncta per cell, as well as the sum of pixels from fluorescent puncta. For each of the presented results, at least 15 individual images were analyzed. (For interpretation of the references to colour in this figure legend, the reader is referred to the web version of this article.)

dynamic light scattering. Due to the poor assembly properties, no LUVs for SM and CER were prepared; lipids used as received. LUVs were stable at pH 3 for several weeks without changing their size distribution (as determined by DLS measurements). In contrast, LUVs nearly instantaneously disassemble at pH below 2.5. We infer that this disassembly is caused by the protonation of their head groups.

5.3. Insulin aggregation

In the lipid-free environment, 400 μM of insulin was dissolved in PBS; solution pH was adjusted to pH 3.0 using concentrated HCl. For Ins:CL, Ins:CER, Ins:PS and Ins:SM, as well as for Ins:PC:CL (1:0.5:0.5) and Ins:PC:CL (1:0.8:0.2), 400 μM of insulin was mixed with an equivalent concentration of the corresponding lipid; solution pH was adjusted to pH 3.0 using concentrated HCl. Next, the solutions were placed in the plate reader (Tecan, Männedorf, Switzerland) and incubated at 37 °C under 510 rpm for 24 h. Although insulin can aggregate forming fibrils at physiological pH, pH 3.0 was chosen in this work because insulin isoelectric point is ~5.3. This drastically lowers protein solubility at pHs above 3.8. At the same time, at pH lower than 3.0, LUVs could be easily disassembled due to protonation of their headgroups.

5.4. Kinetic measurements

Insulin aggregation was monitored using thioflavin T (ThT) fluorescence assay. Briefly, protein samples were mixed with 2 mM of ThT solution and placed in the plate reader (Tecan, Männedorf, Switzerland) where samples were incubated at 37 °C under 510 rpm for 30 h. Fluorescence measurements were taken every 10 min. Excitation wavelength was 450 nm; emission was collected at 488 nm. ThT measurements were done in triplicates.

5.5. AFM imaging

AFM imaging was performed using silicon AFM probes with related parameters force constant 2.7 N/m and resonance frequency 50–80 kHz were purchased from Appnano (Mountain View, CA, USA) on AIST-NT-HORIBA system (Edison, NJ). After 24 h of incubation of insulin (400 μM) with and without lipids at 37 °C under 510 rpm, sample aliquots were diluted with 1xPBS pH 3.0; deposited onto pre-cleaned silicon wafer and dried under a flow of dry nitrogen. Analysis of collected images was performed using AIST-NT software (Edison, NJ, USA).

5.6. AFM-IR

AFM-IR imaging was conducted using a Nano-IR3 system (Bruker, Santa Barbara, CA, USA). The IR source was a QCL laser. Contact-mode AFM tips (ContGB-G AFM probe, NanoAndMore, Watsonville, CA, USA) were used to obtain all spectra and maps. Sample aliquots were diluted with 1xPBS pH 3.0; deposited onto pre-cleaned silicon wafer and dried under a flow of dry nitrogen. Treatment and analysis of collected spectra was performed in Matlab (The Mathworks, Inc. Natick, Massachusetts, USA).

5.7. Circular Dichroism (CD)

After 24 h of sample incubation, samples were diluted to the final concentration of 100 μM using PBS and measured immediately using J-1000 CD spectrometer (Jasco, Easton, MD, USA). Three spectra were collected for each sample within 205–250 nm.

5.8. Attenuated total reflectance Fourier-transform Infrared (ATR-FTIR) spectroscopy

After 24 h of sample incubation, samples were placed onto ATR crystal and dried at room temperature. Spectra were measured using Spectrum 100 FTIR spectrometer (Perkin-Elmer, Waltham, MA, USA). Three spectra were collected from each sample.

5.9. Cell toxicity assays

Mice midbrain N27 cells were grown in RPMI 1640 Medium (Thermo Fisher Scientific, Waltham, MA, USA) with 10 % fetal bovine serum (FBS) (Invitrogen, Waltham, MA, USA) in 96 well-plate (5000 cells per well) at 37 °C under 5 % CO_2. After 24 h, the cells were found to fully adhere to the wells reaching ~70 % confluency. Next, 100 μL of the cell culture was replaced with 100 μL RPMI 1640 Medium with 5 % FBS containing protein samples. Concentration of FBS was decreased from 10 % to 5 % to lower the baseline absorbance level of the control according to the specifications of lactate dehydrogenase (LDH) assay (G1781, Promega, Madison, WI, USA) that was used to determine toxicity of insulin aggregates. Insulin aggregates grown in the presence and absence of lipids (24 h), as well as lipids alone were added to N27 cells to reach the final concentration of 400 μM. After 48 h of incubation, we used CytoTox 96 non-radioactive cytotoxicity assay to determine LDH levels in N27 cells. Absorption measurements were made in plate reader (Tecan, Männedorf, Switzerland) at 490 nm. Every well was measured 25 times in different locations.

In parallel, reactive oxygen species (ROS) assay was performed using the same cell culture. Briefly, ROS reagent (C10422, Invitrogen, Waltham, MA, USA) was added to reach the final concentration of 5 μM and incubated at 37 °C under 5 % CO_2 for 30 min. After the supernatant was removed, cells were washed with PBS and resuspended in 200 μL of PBS in the flow cytometry tubes. Sample measurements were made in Accuri C6 Flow Cytomer (BD, San Jose, CA, USA) using red channel ($\lambda = 633$ nm). Percentages of ROS cells was determined using Acura software.

For JC-1 staining, 1 μL of JC-1 reagent (M34152A, Invitrogen, Waltham, MA, USA) was added to cells and incubated at 37 °C under 5 % CO_2 for 30 min. After the supernatant was removed, cells were washed with PBS and resuspended in 200 μL of PBS in the flow cytometry tubes. Sample measurements were made in Accuri C6 Flow Cytomer (BD, San Jose, CA, USA) using red channel ($\lambda = 633$ nm). Percentages of ROS cells was determined using Accuri software.

5.10. Membrane leakage assay

Three plasmids that code biomarkers Charged multivesicular body protein 1b (Chmp1b - cell membrane repair), Galectin-3 (Gal3 - autophagy) and Transcription factor EB (TFEB - lysosome biogenesis) were used. Plasmids were delivered in HEK 293 T cell using GeneX Plus reagent (ACS-4004, ATCC, Manassas, VA, USA). HET 293 T cells were grown in Dulbecco's Modified Eagle Medium (DMEM) cell medium with 10 % FBS. After 24 h, the cells were found to fully adhere to the wells reaching ~80 % confluency. Transfection was made in DMEM without FBS during 4 h. Next, cell media was replaced on DMEM with 10 % FBS and incubated for 24 h. Protein samples were added to the cells and incubated for 24 h. Fluorescence cell imaging was performed in EVOS M5000 microscope (Thermo Fisher Scientific, Waltham, MA, USA). Chmp1b and TFEB plasmids contain green fluorescence protein and Gal3 contains red fluorescence protein, Fig. S4. Microscopic images reported in Fig. S4 show cells with various numbers of punctata present in each cell. Using these images, we counted number of punctata in cells treated with insulin aggregates grown in the presence and absence of lipids. The number of punctata was reported in the histograms shown in the Fig. 6.

CRediT authorship contribution statement

Conceptualization: MM and DK; Methodology: MM, SR, J-FP and DK; Validation: MM, SR; Data analysis: MM, SR; Investigation: MM, SR, DK; Resources: DK; Writing and editing: all authors.

Declaration of competing interest

Dmitry Kurouski reports financial support was provided by Texas A&M University.

The authors declare no competing financial interests.

Data availability statement

All data described in this manuscript are contained within the manuscript.

Acknowledgement

We are grateful to the US National Institute of General Medical Sciences (D.K.: R35GM142869; J.-P.P.: R01GM110137) and the Cancer Prevention and Research Institute of Texas (J.-P.P.: RP190655) for the provided financial support.

Appendix A. Supplementary data

Supplementary data to this article can be found online at https://doi.org/10.1016/j.bbalip.2022.159247.

References

[1] F. Chiti, C.M. Dobson, Protein misfolding, amyloid formation, and human disease: a summary of progress over the last decade, Annu. Rev. Biochem. 86 (2017) 27–68.
[2] T.P. Knowles, M. Vendruscolo, C.M. Dobson, The amyloid state and its association with protein misfolding diseases, Nat. Rev. 15 (2014) 384–396.
[3] M.G. Iadanza, M.P. Jackson, E.W. Hewitt, N.A. Ranson, S.E. Radford, A new era for understanding amyloid structures and disease, Nat. Rev. Mol. Cell Biol. 19 (2018) 755–773.
[4] S.W. Chen, S. Drakulic, E. Deas, M. Ouberai, F.A. Aprile, R. Arranz, S. Ness, C. Roodveldt, T. Guilliams, E.J. De-Genst, D. Klenerman, N.W. Wood, T. P. Knowles, C. Alfonso, G. Rivas, A.Y. Abramov, J.M. Valpuesta, C.M. Dobson, N. Cremades, Structural characterization of toxic oligomers that are kinetically trapped during alpha-synuclein fibril formation, Proc. Natl. Acad. Sci. U. S. A. 112 (2015) E1994–E2003.
[5] T. Dou, L. Zhou, D. Kurouski, Unravelling the structural organization of individual alpha-synuclein oligomers grown in the presence of phospholipids, J. Phys. Chem. Lett. 12 (2021) 4407–4414.
[6] L. Pieri, K. Madiona, R. Melki, Structural and functional properties of prefibrillar α-synuclein oligomers, Sci. Rep. 6 (2016) 24526.
[7] N. Cremades, S.I. Cohen, E. Deas, A.Y. Abramov, A.Y. Chen, A. Orte, M. Sandal, R. W. Clarke, P. Dunne, F.A. Aprile, C.W. Bertoncini, N.W. Wood, T.P. Knowles, C. M. Dobson, D. Klenerman, Direct observation of the interconversion of normal and toxic forms of alpha-synuclein, Cell 149 (2012) 1048–1059.
[8] M.M. Apetri, N.C. Maiti, M.G. Zagorski, P.R. Carey, V.E. Anderson, Secondary structure of alpha-synuclein oligomers: characterization by Raman and atomic force microscopy, J. Mol. Biol. 355 (2006) 63–71.
[9] E.I. O'Leary, J.C. Lee, Interplay between alpha-synuclein amyloid formation and membrane structure, Biochim. Biophy.s Acta Proteins Proteom. 1867 (2019) 483–491.
[10] D. Kurouski, R.P. Van Duyne, I.K. Lednev, Exploring the structure and formation mechanism of amyloid fibrils by Raman spectroscopy: a review, Analyst 140 (2015) 4967–4980.
[11] D.P. Hong, S. Han, A.L. Fink, V.N. Uversky, Characterization of the non-fibrillar alpha-synuclein oligomers, Prot. Pept. Lett. 18 (2011) 230–240.
[12] A.K. Paravastu, I. Qahwash, R.D. Leapman, S.C. Meredith, R. Tycko, Seeded growth of beta-amyloid fibrils from Alzheimer's brain-derived fibrils produces a distinct fibril structure, Proc. Natl. Acad. Sci. U. S. A. 106 (2009) 7443–7448.
[13] B. Li, P. Ge, K.A. Murray, P. Sheth, M. Zhang, G. Nair, M.R. Sawaya, W.S. Shin, D. R. Boyer, S. Ye, D.S. Eisenberg, Z.H. Zhou, L. Jiang, Cryo-EM of full-length alpha-synuclein reveals fibril polymorphs with a common structural kernel, Nat. Commun. 9 (2018) 3609.
[14] R. Guerrero-Ferreira, N.M. Taylor, D. Mona, P. Ringler, M.E. Lauer, R. Riek, M. Britschgi, H. Stahlberg, Cryo-EM structure of alpha-synuclein fibrils, elife 7 (2018).
[15] R. Tycko, Solid-state NMR studies of amyloid fibril structure, Annu. Rev. Phys. Chem. 62 (2011) 279–299.
[16] P.H. Nguyen, A. Ramamoorthy, B.R. Sahoo, J. Zheng, P. Faller, J.E. Straub, L. Dominguez, J.E. Shea, N.V. Dokholyan, A. De Simone, B. Ma, R. Nussinov, S. Najafi, S.T. Ngo, A. Loquet, M. Chiricotto, P. Ganguly, J. McCarty, M.S. Li, C. Hall, Y. Wang, Y. Miller, S. Melchionna, B. Habenstein, S. Timr, J. Chen, B. Hnath, B. Strodel, R. Kayed, S. Lesne, G. Wei, F. Sterpone, A.J. Doig, P. Derreumaux, Amyloid oligomers: a joint experimental/computational perspective on Alzheimer's disease, Parkinson's disease, type II diabetes, and amyotrophic lateral sclerosis, Chem. Rev. 121 (2021) 2545–2647.
[17] E.E. Cawood, T.K. Karamanos, A.J. Wilson, S.E. Radford, Visualizing and trapping transient oligomers in amyloid assembly pathways, Biophys. Chem. 268 (2021), 106505.
[18] G.J. Morgan, Transient disorder along pathways to amyloid, Biophys. Chem. 281 (2022), 106711.
[19] S. Barghorn, V. Nimmrich, A. Striebinger, C. Krantz, P. Keller, B. Janson, M. Bahr, M. Schmidt, R.S. Bitner, J. Harlan, E. Barlow, U. Ebert, H. Hillen, Globular amyloid beta-peptide oligomer - a homogenous and stable neuropathological protein in Alzheimer's disease, J. Neurochem. 95 (2005) 834–847.
[20] M. Serra-Batiste, M. Ninot-Pedrosa, M. Bayoumi, M. Gairi, G. Maglia, N. Carulla, Abeta42 assembles into specific beta-barrel pore-forming oligomers in membrane-mimicking environments, Proc. Natl. Acad. Sci. U. S. A. 113 (2016) 10866–10871.
[21] S. Banerjee, Z. Sun, E.Y. Hayden, D.B. Teplow, Y.L. Lyubchenko, Nanoscale dynamics of amyloid beta-42 oligomers as revealed by high-speed atomic force microscopy, ACS Nano 11 (2017) 12202–12209.
[22] T. Watanabe-Nakayama, K. Ono, M. Itami, R. Takahashi, D.B. Teplow, M. Yamada, High-speed atomic force microscopy reveals structural dynamics of amyloid beta1-42 aggregates, Proc. Natl. Acad. Sci. U. S. A. 113 (2016) 5835–5840.
[23] S. Rizevsky, D. Kurouski, Nanoscale structural organization of insulin fibril polymorphs revealed by atomic force microscopy-infrared spectroscopy (AFM-IR), Chembiochem 21 (2020) 481–485.
[24] F.S. Ruggeri, J. Charmet, T. Kartanas, Q. Peter, S. Chia, J. Habchi, C.M. Dobson, M. Vendruscolo, T.P.J. Knowles, Microfluidic deposition for resolving single-molecule protein architecture and heterogeneity, Nat. Commun. 9 (2018) 3890.
[25] F.S. Ruggeri, P. Flagmeier, J.R. Kumita, G. Meisl, D.Y. Chirgadze, M. N. Bongiovanni, T.P.J. Knowles, C.M. Dobson, The influence of pathogenic mutations in alpha-synuclein on biophysical and structural characteristics of amyloid fibrils, ACS Nano 14 (2020) 5213–5222.
[26] F.S. Ruggeri, G. Longo, S. Faggiano, E. Lipiec, A. Pastore, G. Dietler, Infrared nanospectroscopy characterization of oligomeric and fibrillar aggregates during amyloid formation, Nat. Commun. 6 (2015) 7831.
[27] L. Zhou, D. Kurouski, Structural characterization of individual alpha-synuclein oligomers formed at different stages of protein aggregation by atomic force microscopy-infrared spectroscopy, Anal. Chem. 92 (2020) 6806–6810.
[28] T. Deckert-Gaudig, E. Kämmer, V. Deckert, Tracking of nanoscale structural variations on a single amyloid fibril tip-enhanced raman scattering, J. Biophotonics 5 (2012) 215–219.
[29] A.V. Krasnoslobodtsev, T. Deckert-Gaudig, Y. Zhang, V. Deckert, Y. L. Lyubchenko, Polymorphism of amyloid fibrils formed by a peptide from the yeast prion protein Sup35: AFM and tip-enhanced Raman scattering studies, Ultramicroscopy 165 (2016) 26–33.
[30] D. Kurouski, T. Deckert-Gaudig, V. Deckert, I.K. Lednev, Structure and composition of insulin fibril surfaces probed by TERS, J. Am. Chem. Soc. 134 (2012) 13323–13329.
[31] D. Kurouski, T. Deckert-Gaudig, V. Deckert, I.K. Lednev, Surface characterization of insulin protofilaments and fibril polymorphs using tip-enhanced Raman spectroscopy (TERS), Biophys. J. 106 (2014) 263–271.
[32] E. Lipiec, D. Perez-Guaita, J. Kaderli, B.R. Wood, R. Zenobi, Direct nanospectroscopic verification of the amyloid aggregation pathway, Angew. Chem. 57 (2018) 8765–8770.
[33] Y. Zhang, M. Hashemi, Z. Lv, B. Williams, K.I. Popov, N.V. Dokholyan, Y. L. Lyubchenko, High-speed atomic force microscopy reveals structural dynamics of alpha-synuclein monomers and dimers, J. Chem. Phys. 148 (2018), 123322.
[34] A. Kakinen, Y. Xing, N.Hegoda Arachchi, I. Javed, L. Feng, A. Faridi, A.M. Douek, Y. Sun, J. Kaslin, T.P. Davis, M.J. Higgins, F. Ding, P.C. Ke, Single-molecular heteroamyloidosis of human islet amyloid polypeptide, Nano Lett. 19 (2019) 6535–6546.
[35] L. Wei, P. Jiang, W. Xu, H. Li, H. Zhang, L. Yan, M.B. Chan-Park, X.W. Liu, K. Tang, Y. Mu, K. Pervushin, The molecular basis of distinct aggregation pathways of islet amyloid polypeptide, J. Biol. Chem. 286 (2011) 6291–6300.
[36] A. Dazzi, F. Glotin, R. Carminati, Theory of infrared nanospectroscopy by photothermal induced resonance, J. Appl. Phys. 107 (2010), 124519.
[37] A. Dazzi, C.B. Prater, AFM-IR: technology and applications in nanoscale infrared spectroscopy and chemical imaging, Chem. Rev. 117 (2017) 5146–5173.
[38] D. Kurouski, A. Dazzi, R. Zenobi, A. Centrone, Infrared and Raman chemical imaging and spectroscopy at the nanoscale, Chem. Soc. Rev. 49 (2020) 3315–3347.
[39] A.M. Katzenmeyer, V. Aksyuk, A. Centrone, Nanoscale infrared spectroscopy: improving the spectral range of the photothermal induced resonance technique, Anal. Chem. 85 (2013) 1972–1979.
[40] A.M. Katzenmeyer, G. Holland, K. Kjoller, A. Centrone, Absorption spectroscopy and imaging from the visible through mid-infrared with 20 nm resolution, Anal. Chem. 87 (2015) 3154–3159.
[41] F.S. Ruggeri, B. Mannini, R. Schmid, M. Vendruscolo, T.P.J. Knowles, Single molecule secondary structure determination of proteins through infrared absorption nanospectroscopy, Nat. Commun. 11 (2020) 2945.
[42] F. Lu, M.Z. Jin, M.A. Belkin, Tip-enhanced infrared nanospectroscopy via molecular expansion force detection, Nat. Photon. 8 (2014) 307–312.
[43] F.S. Ruggeri, F. Benedetti, T.P.J. Knowles, H.A. Lashuel, S. Sekatskii, G. Dietler, Identification and nanomechanical characterization of the fundamental single-strand protofilaments of amyloid alpha-synuclein fibrils, Proc. Natl. Acad. Sci. U. S. A. 115 (2018) 7230–7235.

[44] F.S. Ruggeri, S. Vieweg, U. Cendrowska, G. Longo, A. Chiki, H.A. Lashuel, G. Dietler, Nanoscale studies link amyloid maturity with polyglutamine diseases onset, Sci. Rep. 6 (2016) 31155.
[45] G. Ramer, F.S. Ruggeri, A. Levin, T.P.J. Knowles, A. Centrone, Determination of polypeptide conformation with nanoscale resolution in water, ACS Nano 12 (2018) 6612–6619.
[46] C. Farber, J. Li, E. Hager, R. Chemelewski, J. Mullet, A.Y. Rogachev, D. Kurouski, Complementarity of Raman and infrared spectroscopy for structural characterization of plant epicuticular waxes, ACS Omega 4 (2019) 3700–3707.
[47] C. Farber, R. Wang, R. Chemelewski, J. Mullet, D. Kurouski, Nanoscale structural organization of plant epicuticular wax probed by atomic force microscope infrared spectroscopy, Anal. Chem. 91 (2019) 2472–2479.
[48] A. Dazzi, Photothermal induced resonance. Application to infrared spectromicroscopy, in: S. Volz (Ed.), Thermal Nanosystems and Nanomaterials, vol. 118, Springer, Berlin, 2009, pp. 469–503.
[49] D. Perez-Guaita, K. Kochan, M. Batty, C. Doerig, J. Garcia-Bustos, S. Espinoza, D. McNaughton, P. Heraud, B.R. Wood, Multispectral atomic force microscopy-infrared nano-imaging of malaria infected red blood cells, Anal. Chem. 90 (2018) 3140–3148.
[50] J. Mathurin, E. Dartois, T. Pino, C. Engrand, J. Duprat, A. Deniset-Besseau, F. Borodnics, C. Sandt, A. Dazzi, Nanometer scale infrared chemical imaging of organic matter in ultracarbonaceous Antarctic micrometeorites (UCAMM), Astron.Astrophys. (2019), https://doi.org/10.1051/0004-6361/201833957.
[51] A. Dazzi, R. Prazeres, F. Glotin, J.M. Ortega, M. Al-Sawaftah, M. de Frutos, Chemical mapping of the distribution of viruses into infected bacteria with a photothermal method, Ultramicroscopy 108 (2008) 635–641.
[52] C. Mayet, A. Deniset-Besseau, R. Prazeres, J.M. Ortega, A. Dazzi, Analysis of bacterial polyhydroxybutyrate production by multimodal nanoimaging, Biotechnol. Adv. 31 (2013) 369–374.
[53] K. Kochan, D. Perez-Guaita, J. Pissang, J.H. Jiang, A.Y. Peleg, D. McNaughton, P. Heraud, B.R. Wood, In vivo atomic force microscopy-infrared spectroscopy of bacteria, J. R.Soc. Interface 15 (2018), 20180115.
[54] K. Wieland, G. Ramer, V.U. Weiss, G. Allmaier, B. Lendl, A. Centrone, Nanoscale chemical imaging of individual chemotherapeutic cytarabine-loaded liposomal nanocarriers, Nano Res. 12 (2019) 197–203.
[55] E. Strelcov, Q. Dong, T. Li, J. Chae, Y. Shao, Y. Deng, A. Gruverman, J. Huang, A. Centrone, CH3NH3PbI3 perovskites: ferroelasticity revealed, Sci. Adv. 3 (2017), e1602165.
[56] R. Cataldi, S. Chia, K. Pisani, F.S. Ruggeri, C.K. Xu, T. Sneideris, M. Perni, S. Sarwat, P. Joshi, J.R. Kumita, S. Linse, J. Habchi, T.P.J. Knowles, B. Mannini, C.M. Dobson, M. Vendruscolo, A dopamine metabolite stabilizes neurotoxic amyloid-beta oligomers, Commun. Biol. 4 (2021) 19.
[57] F. Vosough, A. Barth, Characterization of homogeneous and heterogeneous amyloid-beta42 oligomer preparations with biochemical methods and infrared spectroscopy reveals a correlation between infrared spectrum and oligomer size, ACS Chem. Neurosci. 12 (2021) 473–488.
[58] Y. Jinsmaa, P. Sullivan, Y. Sharabi, D.S. Goldstein, DOPAL is transmissible to and oligomerizes alpha-synuclein in human glial cells, Auton. Neurosci. 194 (2016) 46–51.
[59] N.P. Alza, P.A. Iglesias Gonzalez, M.A. Conde, R.M. Uranga, G.A. Salvador, Lipids at the crossroad of alpha-synuclein function and dysfunction: biological and pathological implications, Front. Cell. Neurosci. 13 (2019) 175.
[60] C. Galvagnion, The role of lipids interacting with -synuclein in the pathogenesis of Parkinson's disease, J. Parkinsons Dis. 7 (2017) 433–450.
[61] C. Galvagnion, J.W. Brown, M.M. Ouberai, P. Flagmeier, M. Vendruscolo, A. K. Buell, E. Sparr, C.M. Dobson, Chemical properties of lipids strongly affect the kinetics of the membrane-induced aggregation of alpha-synuclein, Proc. Natl. Acad. Sci. U. S. A. 113 (2016) 7065–7070.
[62] X. Zhang, J.R. St Clair, E. London, D.P. Raleigh, Islet amyloid polypeptide membrane interactions: effects of membrane composition, Biochemistry 56 (2017) 376–390.
[63] N.A. Avdulov, S.V. Chochina, U. Igbavboa, C.S. Warden, A.V. Vassiliev, W. G. Wood, Lipid binding to amyloid beta-peptide aggregates: preferential binding of cholesterol as compared with phosphatidylcholine and fatty acids, J. Neurochem. 69 (1997) 1746–1752.
[64] D. Kurouski, T. Postiglione, T. Deckert-Gaudig, V. Deckert, I.K. Lednev, Amide I vibrational mode suppression in surface (SERS) and tip (TERS) enhanced Raman spectra of protein specimens, Analyst 138 (2013) 1665–1673.
[65] A. D'Souza, J.D. Theis, J.A. Vrana, F. Buadi, A. Dispenzieri, A. Dogan, Localized insulin-derived amyloidosis: a potential pitfall in the diagnosis of systemic amyloidosis by fat aspirate, Am. J. Hematol. 87 (2012) E131–E132.
[66] Y. Gupta, G. Singla, R. Singla, Insulin-derived amyloidosis, IndianJ. Endocrinol. Metab. 19 (2015) 174–177.
[67] Y. Shikama, J. Kitazawa, N. Yagihashi, O. Uehara, Y. Murata, N. Yajima, R. Wada, S. Yagihashi, Localized amyloidosis at the site of repeated insulin injection in a diabetic patient, Intern. Med. 49 (2010) 397–401.
[68] Y. Miller, Advancements and future directions in research of the roles of insulin in amyloid diseases, Biophys. Chem. 281 (2022), 106720.
[69] K. Iwaya, T. Zako, J. Fukunaga, K.M. Sörgjerd, K. Ogata, K. Kogure, H. Kosano, M. Noritake, M. Maeda, Y. Ando, Y. Katsura, T. Nagase, Toxicity of insulin-derived amyloidosis: a case report, BMC Endocr. Dis. 19 (1991) 61.
[70] D. Fitzner, J.M. Bader, H. Penkert, C.G. Bergner, M. Su, M.T. Weil, M.A. Surma, M. Mann, C. Klose, M. Simons, Cell-type- and brain-region-resolved mouse brain lipidome, Cell Rep. 32 (2020), 108132.
[71] G. van Meer, D.R. Voelker, G.W. Feigenson, Membrane lipids: where they are and how they behave, Nat. Rev. Mol. Cell. Biol. 9 (2008) 112–124.
[72] E. Fahy, S. Subramaniam, R.C. Murphy, M. Nishijima, C.R. Raetz, T. Shimizu, F. Spener, G. van Meer, M.J. Wakelam, E.A. Dennis, Update of the LIPID MAPS comprehensive classification system for lipids, J. Lipid Res. 50 (Suppl) (2009) S9–S14.
[73] D.M. Michaelson, G. Barkai, Y. Barenholz, Asymmetry of lipid organization in cholinergic synaptic vesicle membranes, Biochem. J. 211 (1983) 155–162.
[74] D. Kurouski, H. Luo, V. Sereda, F.T. Robb, I.K. Lednev, Rapid degradation kinetics of amyloid fibrils under mild conditions by an archaeal chaperonin, Biochem. Biophys. Res. Commun. 422 (2012) 97–102.
[75] A. De Simone, M. Naldi, D. Tedesco, A. Milelli, M. Bartolini, L. Davani, D. Widera, M.L. Dallas, V. Andrisano, Investigating in vitro amyloid peptide 1–42 aggregation: impact of higher molecular weight stable adducts, ACS Omega 4 (2019) 12308–12318.
[76] D. Kurouski, R.A. Lombardi, R.K. Dukor, I.K. Lednev, L.A. Nafie, Direct observation and pH control of reversed supramolecular chirality in insulin fibrils by vibrational circular dichroism, Chem. Commun. 46 (2010) 7154–7156.
[77] A. Barth, Infrared spectroscopy of proteins, Biochim. Biophys. Acta 1767 (2007) 1073–1101.
[78] R. Sarroukh, E. Goormaghtigh, J.M. Ruysschaert, V. Raussens, ATR-FTIR: a "rejuvenated" tool to investigate amyloid proteins, Biochim. Biophys. Acta 2013 (1828) 2328–2338.
[79] N.B. Colthup, L.H. Daly, S.E. Wiberley, Introduction to Infrared and Raman Spectroscopy, Academic Press, 1990.
[80] T. Dou, Z. Li, J. Zhang, A. Evilevitch, D. Kurouski, Nanoscale structural characterization of individual viral particles using atomic force microscopy infrared spectroscopy (AFM-IR) and tip-enhanced Raman spectroscopy (TERS), Anal. Chem. 92 (2020) 11297–11304.
[81] C. Galvagnion, A.K. Buell, G. Meisl, T.C. Michaels, M. Vendruscolo, T.P. Knowles, C.M. Dobson, Lipid vesicles trigger alpha-synuclein aggregation by stimulating primary nucleation, Nat. Chem. Biol. 11 (2015) 229–234.
[82] S. Srinivasan, S. Patke, Y. Wang, Z. Ye, J. Litt, S.K. Srivastava, M.M. Lopez, D. Kurouski, I.K. Lednev, R.S. Kane, W. Colon, Pathogenic serum amyloid a 1.1 shows a long oligomer-rich fibrillation lag phase contrary to the highly amyloidogenic non-pathogenic SAA2.2, J. Biol. Chem. 288 (2013) 2744–2755.
[83] E. Wesén, G.D.M. Jeffries, M.M. Dzebo, E.K. Esbjörner, Endocytic uptake of monomeric amyloid-β peptides is clathrin- and dynamin-independent and results in selective accumulation of Aβ(1–42) compared to Aβ(1–40), Sci. Rep. 7 (2017) 2021.
[84] R.W. Choy, Z. Cheng, R. Schekman, Amyloid precursor protein (APP) traffics from the cell surface via endosomes for amyloid beta (Abeta) production in the trans-Golgi network, Proc. Natl. Acad. Sci. U. S. A. 109 (2012) E2077–E2082.
[85] H.M. Kondow-McConaghy, N. Muthukrishnan, A. Erazo-Oliveras, K. Najjar, R. L. Juliano, J.P. Pellois, Impact of the endosomal escape activity of cell-penetrating peptides on the endocytic pathway, ACS Chem. Biol. 15 (2020) 2355–2363.
[86] M.L. Skowyra, P.H. Schlesinger, T.V. Naismith, P.I. Hanson, Triggered recruitment of ESCRT machinery promotes endolysosomal repair, Science 360 (2018).
[87] M. Radulovic, K.O. Schink, E.M. Wenzel, V. Nahse, A. Bongiovanni, F. Lafont, H. Stenmark, ESCRT-mediated lysosome repair precedes lysophagy and promotes cell survival, EMBO J. 37 (2018).
[88] I. Paz, M. Sachse, N. Dupont, J. Mounier, C. Cederfur, J. Enninga, H. Leffler, F. Poirier, M.C. Prevost, F. Lafont, P. Sansonetti, Galectin-3, a marker for vacuole lysis by invasive pathogens, Cell. Microbiol. 12 (2010) 530–544.
[89] C. Settembre, C. Di Malta, V.A. Polito, M. Garcia Arencibia, F. Vetrini, S. Erdin, S. U. Erdin, T. Huynh, D. Medina, P. Colella, M. Sardiello, D.C. Rubinsztein, A. Ballabio, TFEB links autophagy to lysosomal biogenesis, Science 332 (2011) 1429–1433.
[90] M. Sardiello, M. Palmieri, A. di Ronza, D.L. Medina, M. Valenza, V.A. Gennarino, C. Di Malta, F. Donaudy, V. Embrione, R.S. Polishchuk, S. Banfi, G. Parenti, E. Cattaneo, A. Ballabio, A gene network regulating lysosomal biogenesis and function, Science 325 (2009) 473–477.
[91] D.L. Medina, S. Di Paola, I. Peluso, A. Armani, D. De Stefani, R. Venditti, S. Montefusco, A. Scotto-Rosato, C. Prezioso, A. Forrester, C. Settembre, W. Wang, Q. Gao, H. Xu, M. Sandri, R. Rizzuto, M.A. De Matteis, A. Ballabio, Lysosomal calcium signalling regulates autophagy through calcineurin and TFEB, Nat. Cell Biol. 17 (2015) 288–299.
[92] M. Kinoshita, E. Kakimoto, M.S. Terakawa, Y. Lin, T. Ikenoue, M. So, T. Sugiki, A. Ramamoorthy, Y. Goto, Y.H. Lee, Model membrane size-dependent amyloidogenesis of Alzheimer's amyloid-beta peptides, Phys. Chem. Chem. Phys. 19 (2017) 16257–16266.
[93] M.S. Terakawa, Y. Lin, M. Kinoshita, S. Kanemura, D. Itoh, T. Sugiki, M. Okumura, A. Ramamoorthy, Y.H. Lee, Impact of membrane curvature on amyloid aggregation, Biochim. Biophys. Acta Biomembr. 2018 (1860) 1741–1764.
[94] M.S. Terakawa, H. Yagi, M. Adachi, Y.H. Lee, Y. Goto, Small liposomes accelerate the fibrillation of amyloid beta (1–40), J. Biol. Chem. 290 (2015) 815–826.
[95] T. Viennet, M.M. Wordehoff, B. Uluca, C. Poojari, H. Shaykhalishahi, D. Willbold, B. Strodel, H. Heise, A.K. Buell, W. Hoyer, M. Etzkorn, Structural insights from lipid-bilayer nanodiscs link alpha-synuclein membrane-binding modes to amyloid fibril formation, Commun. Biol. 1 (2018) 44.
[96] B.I. Giasson, I.V. Murray, J.Q. Trojanowski, V.M. Lee, A hydrophobic stretch of 12 amino acid residues in the middle of alpha-synuclein is essential for filament assembly, J. Biol. Chem. 276 (2001) 2380–2386.
[97] K. Ueda, H. Fukushima, E. Masliah, Y. Xia, A. Iwai, M. Yoshimoto, D.A. Otero, J. Kondo, Y. Ihara, T. Saitoh, Molecular cloning of cDNA encoding an

unrecognized component of amyloid in Alzheimer disease, Proc. Natl. Acad. Sci. U. S. A. 90 (1993) 11282–11286.
[98] T. Dou, D. Kurouski, Phosphatidylcholine and phosphatidylserine uniquely modify the secondary structure of alpha-synuclein oligomers formed in their presence at the early stages of protein aggregation, ACS Chem. Neurosci. 13 (2022) 2380–2385.
[99] S. Rizevsky, M. Matveyenka, D. Kurouski, Nanoscale structural analysis of a lipid-driven aggregation of insulin, J. Phys. Chem. Lett. 13 (2022) 2467–2473.
[100] M. Matveyenka, S. Rizevsky, D. Kurouski, Unsaturation in the fatty acids of phospholipids drastically alters the structure and toxicity of insulin aggregates grown in their presence, J. Phys. Chem. Lett. (2022) 4563–4569.
[101] M. Matveyenka, S. Rizevsky, D. Kurouski, The degree of unsaturation of fatty acids in phosphatidylserine alters the rate of insulin aggregation and the structure and toxicity of amyloid aggregates, FEBS Lett. 596 (2022) 1424–1433.
[102] M. Matveyenka, S. Rizevsky, D. Kurouski, Amyloid aggregates exert cell toxicity causing irreversible damages in the endoplasmic reticulum, Biochim. Biophys. Acta Mol. basis Dis. 1868 (2022), 166485.
[103] C. Galvagnion, A.K. Buell, G. Meisl, T.C.T. Michaels, M. Vendruscolo, T.P. J. Knowles, C.M. Dobson, Lipid vesicles trigger α-synuclein aggregation by stimulating primary nucleation, Nat. Chem. Biol. 11 (2015) 229–234.